DOE/SF/20717--T1

Final Technical Report

Department of Energy Contract

DE-FG03-95SF20717

Principal Investigator:

Charles F. Hooper, Jr.

MASTER

DISCLAIMER

Final Technical Report for the Period

4/17/95 - 9/30/97

Charles F. Hooper, Jr.

March 1998

Work Performed Under Contract

DE-FG03-95SF20712

U.S. Department of Energy

DE-FG03-95SF20712
(4/17/95 - 9/30/97)

The body of this report is contained in the three attached documents which deal with plasma spectroscopy of laser-produced plasmas. In the appendix A we present a discussion of plasma line broadening with our emphasis on the effects of accounting for ion-dynamic corrections. In appendix B we present more research related to ion-dynamic corrections. Appendix C addresses the use of high opacity Krypton lines to diagnose high temperature implosions, and provides additional detail about the effects of ion dynamics.

reprint removed.

Spectroscopic Analysis of Hot Dense Plasmas: A Focus on Ion Dynamics

Appendix A

Charles F. Hooper, Jr.

DE-FG03-95SF20712

Spectroscopic Analysis of Hot Dense Plasmas: A Focus on Ion Dynamics

C. F. Hooper, Jr., D. A. Haynes, Jr., and D. T. Garber

Department of Physics
University of Florida
Gainesville, FL 32611

R. C. Mancini

Department of Physics
University of Nevada
Reno, NV 89557

Y. T. Lee

Lawrence Livermore National Laboratory
Livermore, CA 94550

D. K. Bradley, J. Delettrez, R. Epstein, and P. A. Jaanimagi

Laboratory for Laser Energetics
University of Rochester
Rochester, NY 14623

Abstract: A brief discussion of the standard theory of line broadening is presented together with an analysis of selected laser driven implosion experiments. The effect of improved theoretical procedures on experimental analysis is discussed. In particular, we consider the combined effects of ion dynamics and opacity on line profiles used in the analysis of these plasmas. The experiments discussed were performed at the University of Rochester Laboratory for Laser Energetics (LLE). The results presented in this paper illustrate the usefulness of plasma line broadening in diagnosing hot dense plasmas and in understanding fundamental plasma processes.

I. Introduction

For two decades, high power lasers have been used to implode microballoons filled with gasses such as neon, argon, deuterium, or mixtures of deuterium and argon. These implosions have generated high-temperature ($\approx$ 1 keV) and high density ($\approx 10^{23}$/cc-10^{25}/cc) plasmas.

As a result of these experiments we are able to observe the radiative properties of highly charged ions in the presence of a variety of strongly coupled plasmas (Griem 1992 and references therein). Spectral radiation observed from these experiments is frequently in the x-ray region and the radiative properties are greatly influenced by plasma effects. In section II of this paper we will discuss the theoretical techniques employed to interpret these spectra and will describe two sets of implosion experiments. In section III we will list some conclusions.

II. Theory and Experiment

A. Theoretical considerations

1. Plasma microfield effects and Stark splitting

If an isolated hydrogen atom or hydrogenic ion is raised to its first excited electronic state it will subsequently return to its ground state with the emission of a photon. A collection of non-interacting excited atoms or ions will radiate one photon per radiator and will produce an intensity distribution $I(\omega)$, as illustrated in Figure 1. If these excited hydrogenic atoms/ions are placed in external electric field, the energy-level structure and resulting intensity will be altered by the familiar Stark effect, as illustrated in Figure 2. Such an electric field could be generated by a static configuration of ions in a plasma, in which case it is called an ion microfield.

Next suppose that we place our radiating ions in a plasma where the ions are assumed to create a static microfield and where each transition is broadenend by dynamic electrons perturbing the individual states; then, if the radiating ion is Ar^{+17}, we find, for two different microfield values, the line profiles are as pictured in Figure 3. ϵ is defined to be $\frac{E}{E_0}$ where E_0 is defined by the expression

$$E_0 = \frac{e}{R_0^2}$$

and

$$R_0 = (\frac{3}{4\pi n_e})^{\frac{1}{3}}.$$

These figures illustrate the effect of a given ion microfield on the intensity patern. Of course in a real plasma each radiator would generally experience a different static ion microfield and hence the final line profile would involve a weighted sum over all values of ϵ. Plasma line broadening theory has been developed to calculate spectral line profiles characteristic of radiators immersed in the plasma environment [see *e.g.*, Griem 1974].

2. Plasma line broadening theory

The "standard theory" of line broadening which is usually employed in practical calculations uses the static ion approximation, in which the plasma ions are treated as static during the radiative lifetime, while the plasma electrons are considered to be dynamic. The ions produce a statistical distribution of ion microfields at the positions of the radiators in the plasma. The calculation of such a distribution is detailed in the literature [Hooper 1966; Hooper 1968; Iglesias *et al.* 1983]. The character of microfield distribution functions is illustrated in the Figure 4. The dynamic plasma electrons are included using a second order quantum mechanical perturbation theory. For both the perturbing ions and electrons the radiator-perturber interaction potentials are treated in the dipole approximation. The expression for the lineshape is given by

$$I(\omega) = \int_0^\infty P(\epsilon) J(\omega, \epsilon) d\epsilon,$$

where $P(\epsilon)$ is the ion microfield distribution function and $J(\omega, \epsilon)$ represents the effect of electron broadening in the presence of an ion microfield ϵ. This lineshape is convolved with a Doppler profile to account for the velocity distribution of the radiators relative to the ovbserver. The lineshape depends on the atomic physics, in particular on whether or not relativistic effects are included. If relativistic atomic physics is used for the Ar Lyman-α line, a much different line shape is obtained. Relativistic effects produce both fine structure splitting and a shift to lower transition energies. For the $2 \rightarrow 1$ transition in Ar^{+17}, the Ar Ly-α line, with $n_e = 5 \times 10^{23}$/cc and $kT_e = 800$eV we arrive at the results for $I(\omega)$ displayed in Figure 5.

The use of Stark broadening of spectral features as a plasma density diagnostic is particularly effective since many such features are very sensitive to changes in density while not particularly sensitive to changes in temperature. However, where several isolated spectral features are observed simultaneously, integrated intensity ratios can supply temperature inferences as well. The density sensitivity of the lineshape is illustrated in the Figure 6, for two different transitions in hydrogen-like Ar. It is clear from a comparison of the plots that for the given temperature and density conditions the lineshape of the $3 \rightarrow 1$ transition, the Ar Lyman-β, is far more density sensitive than the Ly-α line. This is due to the fact that the n=3 level is more sensitive to perturbation than is the n=2 level.

3. Other broadening mechanisms

In addition to the line-broadening mechanisms mentioned above, we must also consider the often competing effects of ion dynamics and opacity. Both of these perturbations are sensitive to variations in plasma constituents.

By varying the composition of the fill gas, we are able to alter systematically the mix of perturbing ions. For cases where the concentration of Ar was small, the static ion approximation employed in the "standard model" becomes suspect, and we implement the BID formalism [Boercker *et al.* 1982] for the inclusion of ion dynamic effects. The

impact of the inclusion of ion dynamics effects on the lineshape is indicated in Figure 7, where the Ar Ly-α is calculated for fixed electron density and temperature, and varying concentration of Ar in D_2. When the concentration of Ar in DD is small, ion dynamic effects significantly modify the static-peak structure. As the relative concentration of Ar rises, the ion dynamics effects become less important, and the effects of opacity begin to significantly alter the lineshape.

In addition to the ion dynamic corrections to our Stark broadening analysis, we regularly include opacity effects on the lineshape. These two effects compete in the sense that for low Ar concentration, ion dynamics is significant and opacity less so. As the concentration of Ar increases, opacity effects increase and ion dynamics broadening decreases. The optical depth, a measure of the importance of opacity effects on the lineshape, is defined as

$$\tau_\omega = \frac{\pi e^2}{mc} \bar{f} \hat{I}(\omega) N_l d; \tag{7}$$

where $\bar{f}$ is the effective oscillator strength for the transition of interest, the circumflex denotes area-normalization with respect to the frequency variable $\frac{\omega}{2\pi}$, N_l the number density of ions in the lower states of the transition, and d is the average chord length in the plasma. In Figure 8, we show the effect of opacity broadening on the Ar He-β line in several approximations. Note that when both ion dynamics and opacity effects are included the optical depth at line center, τ_0, is reduced from 0.66 (static ion approximation) to 0.59 (dynamic ion approximation).

In the following analyses of experimental data the theoretical requirements are demanding, especially the need to include perhaps thousands of atomic states [Cowan 1981]. Our procedure [Woltz and Hooper 1988; Mancini *et al.* 1991] for dealing with these complicated physical situations has the modular form indicated in Figure 9, where specialized codes produce the input for the line broadening code.

B. Experiments and analysis

The experiments that we will discuss in this section involve implosions of gas-filled microballoons performed at the University of Rochester Laboratory for Laser Energetics (LLE). Although these experiments generally involve a variety of diagnostics, our discussion will concentrate on theoretical analysis of time-integrated and time-resolved X-ray spectra.

Before we compare our theoretical spectra to experimental data, we convolve our theoretical profiles with an instumental response function. Also, since our theory treats only bound-bound transitions, we must subtract the background emission due to free-free and free-bound transitions from the experimental data. In addition to simple estimates, spectral analysis programs, such as ROBFIT [Coldwell & Bamford 1991], exist which can be used to more accurately determine the background.

1. 1985 LLE experiments

Given the possibility that Stark broadening analysis of K-shell (H- and He-like) spectra might not always be possible, these experiments were designed to study the feasibility of using L-shell X-ray line emission as a density diagnostic. The laser used to perform these experiments was the 24-beam Ω system which has a wavelength of 3500Å, delivering 2000 J in approximately 600 ps. The targets imploded were plastic microballoons filled with an Argon/Krypton mixture (50/50); coated with a 500Å Aluminum sealing layer. Time integrated spectra were recorded on two spectrographs, one dedicated to recording L-shell Krypton spectra ($3 \rightarrow 2$) and the other to recording Argon K-shell spectra. Theoretical analysis was performed using multi-electron radiator line-broadening theory. As a result of our analysis of the n=3 to n=2 transitions in the Krypton spectra, we determined that these lines were not density sensitive in the 10^{23}/cc to 10^{24}/cc density range and hence were not useful as a density diagnostic.

However, in Figure 10, we see that the spectrograph which was calibrated to record

spectra from hydrogenic and helium-like Argon lines also detected L-shell Krypton line spectra due $4 \rightarrow 2$ transitions. These lines did prove to be density sensitive. Figure 11 illustrates this density sensitivity for n=4 to n=2 transitions in Li-like Krypton. A comparison of our theoretical fit to the part of the spectrum in Figure 10 corresponding to transitions in Li-like and Be-like Ar is shown in Figure 12. The agreement with experiment is quite good except for some differences in intensity, especially in the higher energy range of the spectrum shown. The temperature (1.1 keV) and electron density (1.5×10^{23}/cc) inferences from this fit were consistent with those from our analysis of the Ar K-shell spectra also displayed in Figure 11. Hence we concluded that Stark broadening of L-shell X-ray spectra did indeed offer promise as a plasma-density diagnostic.

2. 1992 LLE experiments

In the fall of 1992, a series of experiments was performed at LLE with the objective of studying the relative importance of ion dynamics and opacity on the observed lineshapes. The 24-beam Ω-laser system used for these experiments operated at 3500 Å, delivering approximately 1000 J in 600 ps and employed beam smoothing techniques. The targets were plastic microballoons with nominal dimensions of 250 microns (diameter) × 6 microns (wall thickness) with a 1000Å Aluminum sealing layer. The fill gas was a mixture of Ar and D_2 with a total pressure of 20 Atm. The partial pressure of Ar varied from 0.01 Atm to 20 Atm (pure Ar). Typical core conditions at stagnation were $n_e = 1 \times 10^{24}\text{cm}^{-3}$, $kT = 900\text{eV}$.

The data taken is displayed as time resolved lineouts of intensity vs. energy. Both Figures 13 and 14 illustrate the data taken as a function of time. As time progresses the spectral lines are broadened and distorted. For instance, in Figure 13 Lineout 5 corresponds to stagnation (maximum density). In our analysis of these spectra we first focus on details of a given line or groups of lines as indicated in Figure 15. In this figure the Ar He-β line is calculated for a fixed temperature and electron density, varying the concentration

of Ar in D_2. As the concentration of Ar increases there is a decrease in the effect of ion dynamics due to the increase in the average perturber mass. Another effect of this trend is the sharpening of peak structure. In general, when ion dynamics is important there is a tendency to broaden the line primarily about the eak structure. Hence, for lines with a substantial central dip, *e.g.*, the Ly-β and He-β, the most obvious effect of ion dynamics is the filling in of the dip. Also noteworthy is the non-linear dependence of the effects of ion dynamics on the concentration of Ar in D_2. By this we mean that as the Argon concentration reaches 10%, the line structure closely resembles that characteristic of the 100% Ar case which, in turn, is very close to the static, 100% Ar case.

Having calculated the lineshapes for the individual transitions of interest, we must combine them with the correct relative intensities to form our theoretical spectrum. A non-LTE kinetics model (Lee 1987) was used to calculate the relative intensities of the lines in the model spectrum. It is important to do the non-LTE modeling to make a realistic estimate of the relative intensities of the satellite lines to their associated resonance lines (Mancini, *et al.* 1992). An important temperature dependence in our model is in the ratio of the Ly-β intensity to the He-β intensity since these lines correspond to different ionization stages. This strong dependence constrains our temperature inferences. Also, the ratios of the intensities of the Li-like satellites to the He-β are temperature sensitive, and, for a given electron density, there is a narrow temperature range where both the intensity of the Ly-β and these satellites are comparable, thus the simultaneous observation of these features is a useful temperature diagnostic in itself.

The non-LTE kinetics calculations were performed initially in the steady-state, optically thin approximation, as we are most interested in analyzing plasmas with low concentrations of Ar, for which the ion motion effects on the lineshapes will be most noticeable. But, however reasonable this proceedure seems, given the small fraction of Ar in D_2 for the plasmas of interest, it leads to a substantial underestimation of the intensity of the Lyman-

β. The transfer of the optically thick ($\tau_0 \sim 10$) He-α line from the core leads to a shift in the ionization balance towards higher ionization stages which results in a diminution of He-like Ar, and an increase in H-like Ar. We included this effect on the resonance lines in our model using an escape factor approximation (Mancini, Joyce, and Hooper 1987). Escape factors were used in the atomic kinetics calculations to account for opacity effects; they affect the computation of excited level populations as well as the total emergent line intensity.

The inclusion of this effect leads to model spectra which can fit simultaneously the relative itensities of the resonance lines as well as the relative intensities of the resonance lines to their attendant satellites. Thus, while opacity has a small impact on the individual lineshapes, it is very important in the determination of the relative intensities.

The sensitivity of our model spectrum to changes in density, and temperature is indicated in Figures 16 and 17. The positions of the centers-of-gravity of the Ar resonance lines are indicated in Figure 16. Also included in our model are five satellites to these resonance lines: the Li-like satellites of the Ar He-β with spectator electron in n=2 (c-o-g 3623eV) and n=3 (3669eV), the He-like satellites of the Ar Ly-β with spectator electron in n=2 (3871eV) and n=3 (3918eV), and the Li-like satellite of the Ar He-γ with spectator electron in n=2 (3797eV). Our model spectrum shows sufficient temperature and density sensitivity to be useful in the analysis of plasmas whose electron temperatures range from 600 to 1200eV, and whose electron densities lie between 5 and $20\times10^{23}\mathrm{cm}^{-3}$

In this section, we discuss the analysis of the x-ray data displayed in Figures 13 and 14. These figures display spectra from shots where the Ar concentration varied from 0.25% Ar in D_2 (Shot A, Figure 13) to 1% Ar in D_2 (Shot B, Figure 14). Even this small difference in Ar concentration causes substantial changes in the relative importance of ion dynamic and opacity effects. For the purposes of this paper, we concentrate on the analysis of lineout 3 from shot A and lineout 3 from shot B.

For these Ar concentrations ion-dynamic-dominated peaks are observed. For the 1% case opacity effects on the lineshapes are also evident. For both implosions, core conditions at stagnation were such that K-shell Ar line emission was easily observeable. Time resolved spectra were recorded using a flat-crystal spectrograph. The instrumental response function is approximated by a Gaussian, whose full width at half maximum is energy dependent, ranging from 3.6eV at 3680eV to 4.4eV at 3935eV.

We now use our model spectrum to analyze the data from lineouts A-3 and B-3. We will concentrate on two aspects of the analysis. First, we will focus on the He-β line and its Li-like satellites. The temperature- and density-sensitivity of this composite feature has been presented previously, in the static-ion optically thin approximation (Mancini, *et al.* 1992). This composite spectral feature, the most prominent feature in all the spectra we consider, best illustrates the importance of both ion dynamics and opacity broadening on the lineshape. Secondly, we will illustrate the utility of our model spectrum by attempting to fit the spectral region from 3500eV to 4100eV for a lineout B-3. Preliminary results from the use of our model spectrum, absent the effects of radiative transfer on the intensity ratios, have been presented previously (Haynes, *et al.* 1995). We will consider the consistency of our fits throughout this spectral region, and test the accuracy of our temperature and density inferences. Before comparison, the model spectrum was convolved with our approximation to the instrumental response function, and a background was subtracted from the experimental spectrum.

The role that ion dynamics plays in the formation of the line emission spectra for low concentrations of Ar in D_2 is indicated in Figure 18, where the He-β + Li-like satellites composite spectrum from lineout 3 of shot A (0.25% Ar in D_2) is compared to our model calculation. In Figure 18a, the effect of opacity on the lineshape is seen to be minimal, as the small concentration of Ar prevents significant redistribution of intensity. Also, for this low concentration of Ar in D_2, opacity does not significantly alter the central dip in

the observed He-β. When the effect of ion dynamics is included (Figure 18b), the dip in our model spectrum is commensurate with the experimental data. Analysis of other lineouts from this shot also reveals that by itself opacity can not substantially fill in central dip in the He-β line; inclusion of ion dynamic effects in the line shape calculation leads consistently to spectra which compare well with the experimental data.

The first three fits in Figure 18 (Static, Static + Opacity, and Dynamic) do not satisfactorily match the experimental data in the range 3550-3600eV. The final fit in Figure 18 (Dynamic + Opacity) includes an estimate of the intensity from a Be-like satellite which is necessary to attain good agreement with the data.

Shot B, with four times the Ar concentration of shot A, allows us to explore the importance of ion dynamics on the lineshape when opacity is not negligible. Figure 19 is similar to Figure 18, in that it compares our model spectra to the He-β + Li-like satellites composite spectral feature from the data. As the concentration of Ar in D_2 increases, the effect of opacity on the lineshape becomes more important, and ion dynamics has less of an effect on the peak structure. Indeed the density inference from this lineout depends on the inclusion of opacity, as well as ion dynamics.

In Figure 19, there is a noticeable discrapency between our calculated spectrum and the experimental data, in the spectral region around 3640eV. There is emission in this region in the data which is not present in our model. While this is the most notable illustration of this discrepency, other lineouts also display greater intensity in this region than our calculations predict. The unaccounted for emission occurs in the vicinity of the blue peak of the n=2 Li-like satellite of the He-β. The observed discrepency is greatest for low density conditions, occuring early in the implosions. We conjecture that non-LTE or time dependent effects or level mixing among the initial manifolds of the Li-like satellites not included in our model may enhance the emission in this region.

Having explored the importance of ion dynamics and opacity on the lineshape, we

turn to an examination of the utility of our model spectrum as a tool for the inference of plasma temperature and density. We model line emission from the spectral region 3550eV to 4000eV, including in our calculation the Ar Ly-β, the Ar He-β, -γ , -δ, and associated satellites.

The density inference is most easily made by fitting the blue wings of the Ar He-β and the Ar Ly-β. These wings are usually less effected by the presence of satellites than the red wings, though care must be taken to include the He-δ line when considering the blue side of the Ly-β. These wings display enough density sensitivity to distinguish between lines emitted from plasmas whose densities differ by a factor of 1.5 in this regime of plasma conditions. Thus, we can distinguish between emission from lineouts characteristic of 5, 8 and $10\times10^{23}\mathrm{cm}^{-3}$.

Given a preliminary density inference, we can fine tune the density dependence while ascertaining the average temperature of the emitting region during a specific time interval. In Figure 20, we fit the spectral region from 3550eV to 4000eV for lineout B-3. The temperature inference from this fit is within 10% of those obtained by separately fitting the region containing only the He-β and its Li-like satellites, and the region containing only the Ly-β, the He-γ and -δ, and their satellites. This degree of consistency is typical of our results for this type of test. This consistency in temperature inference can be attributed to the strong constraints put on the fit by the necessity to reproduce emission emanating from transitions in three different ionization stages in Ar. Indeed, it was just this constraint which led to our appreciation of the importance of the radiative transfer effect on the intensity of the Ly-β relative to the intensities of the other lines in the model. Without the inclusion of this effect, it proved impossible to fit the intensity of the Li-like satellites of the He-β and the Ly-β simultaneously with a single temperature.

III. Conclusions

The results of our comparisons of experimental X-ray spectra and theoretical calculations verify that plasma spectroscopy provides useful diagnostic tools to determine the plasma temperatures and densities that occur in hot dense plasmas. Spectroscopy also allows us to understand how the physical processes that occur in these plasmas influence the resulting spectra. In plasmas where the effect of ion dynamics is important, its inclusion in our theoretical formalism leads not only to better fits to the data but also a better understanding of opacity broadening as well. With new technological developments currently anticipated, or in progress, an even greater range of plasma densities and temperatures will be achieved. These future experiments, observed with improved diagnostics, will continue to challenge our theoretical understanding of the underlying physics.

BOERCKER, D.B. *et al.*1982 Phys. Rev. A, **36**, 2254.

COLDWELL, R.L., and BAMFORD, G.J. 1991 *The Theoery and Operation of Spectral Analysis using ROBFIT*, (New York, American Institute of Physics).

COWAN, R.D. 1981 The Theory of Atomic Structure and Spectra, (Berkely and Los Angeles, Univeristy of California Press).

GRIEM, H.R. 1974 *Spectral Line Broadening By Plasmas*, (New York, Academic Press, Inc.).

GRIEM, H.R. 1992 Phys. Fluids B **4**, 2346.

HAYNES, D.A. *et al.*1995 Rev. Sci. Instrum. **66**, 755.

HOOPER, C.F. 1966 Phys. Rev., **149**, 177.

HOOPER, C.F. 1968 Phys. Rev., **165**, 215.

IGLESIAS, C.A. *et al.*1983 Phys. Rev. A, **28**, 1667.

LEE, Y.T. 1987 J. Quant. Spectrosc. Rad. Trans. **38**, 131.

MANCINI, R.C. *et al.*1991 Comp. Phys. Comm., **63**, 314.

MANCINI, R.C. *et al.*1992 Rev. Sci. Instrum. **63**, 5119.

MANCINI, R.C. *et al.*1987 J. Phys. B **20**, 2975.

WOLTZ, L., and HOOPER, C.F. 1988 Phys. Rev. A, **38**, 4766.

FIGURE CAPTIONS

Figure 1. Diagram of an unperturbed $2 \rightarrow 1$ transition in a one-electron radiator and the spectrum emitted.

Figure 2. Diagram of a $2 \rightarrow 1$ transition in a one-electron radiator perturbed by an external electric field and the spectrum emitted.

Figure 3. Ar Lyman-α tranisition under the influence of two different microfields. $n_e = 5 \times 10^{23}\text{cm}^{-3}$, $kT_e = 800\text{eV}$.

Figure 4. Microfield distribution function, $P(\epsilon)$, for a pure hydrogen-like Ar plasma, $n_e = 5 \times 10^{23}\text{cm}^{-3}$, $kT_e = 800\text{eV}$.

Figure 5. Ar Ly-α without (left) and with (right) relativistic atomic physics. $n_e = 5 \times 10^{23}$/cc and $kT_e = 800\text{eV}$.

Figure 6. Density sensitivity of the Ar Ly-α (left) and -β (right). $kT = 800\text{eV}$.

Figure 7. The effect of ion dynamics on the Ar Ly-α lineshape. Pure Ar plasma (left), 0.25%Ar in DD (right). $n_e = 1 \times 10^{24}\text{cm}^{-3}$, $kT = 800\text{eV}$; static calculation, solid line; dynamic calculation, dotted line.

Figure 8: Ion dynamics and opacity effects on the area normalized Ar He-β lineshape, $n_e = 10 \times 10^{23}\text{cm}^{-3}$, $kT = 900\text{eV}$, 0.25% Ar in D_2, d=25μm.

Figure 9. Diagram illustrating the inputs for MERL, the multi-electron radiator line broadening code.

Figure 10. Experimental spectrum displaying both Ar K-shell lines and $4 \rightarrow 2$ Kr L-shell lines.

Figure 11. Theoretical results for Kr $4 \rightarrow 2$ transitions at various densities.

Figure 12. Comparison of theoretical spectrum to experimental spectrum of Figure 9.

Figure 13: Time resolved lineouts from Shot A (0.25% Ar in D_2). Labels used in text to refer to individual lineouts. Individual lineouts are shifted vertically by an arbitrary amount for display purposes. The five lineouts shown each average over approximately 50ps, and the time intervals over which they average overlap by 25ps with neighboring lineouts.

Figure 14: Time resolved lineouts from Shot B (1% Ar in D_2). Labels used in text to refer to individual lineouts. Individual lineouts are shifted vertically by an arbitrary amount for display purposes. The four lineouts shown each average over approximately 25ps, with no overlap between consecutive time intervals.

Figure 15: Area normalized dynamic Stark broadened Ar He-β lineshapes, calculated for 0.025% (ν = 3.37eV), 1% (ν = 1.66eV), and 17% Ar in D_2 (ν = 0.621eV); $n_e = 5 \times 10^{23}\text{cm}^{-3}$, kT = 900eV.

Figure 16: Density sensitivity of the model spectrum, kT = 900eV, .25% Ar in D_2. The centers of gravity of the Ar resonance lines included in our model are indicated.

Figure 17: Temperature sensitivity of the model spectrum, $n_e = 5 \times 10^{23}\text{cm}^{-3}$, 1% Ar in D_2.

Figure 18: Detail from lineout A-3 (0.25% Ar in D_2) and fits using model spectrum, $n_e = 8 \times 10^{23}\text{cm}^{-3}$, kT = 925eV. Only the fit labeled "Dynamic + Opacity" includes the correction for satellite emission in the 3550-3600eV region, as discussed in the text.

Figure 19: Detail from lineout B-3 (1% Ar in D_2), and fits using model spectrum. Static: $n_e = 8 \times 10^{23}\text{cm}^{-3}$, kT = 875eV; Static + Opacity: $n_e = 5 \times 10^{23}\text{cm}^{-3}$, kT = 840eV; Dynamic: $n_e = 8 \times 10^{23}\text{cm}^{-3}$, kT = 875eV; Dynamic + Opacity: $n_e = 5 \times 10^{23}\text{cm}^{-3}$, kT = 840eV.

Figure 20: Best fit to lineout B-3 (1% Ar in D_2), $n_e = 5 \times 10^{23}\text{cm}^{-3}$, kT = 850eV. The dashed traces are the individual lineprofiles that were added to produce the model

spectrum.

The Effects of Ion Dynamics and Opacity on Stark Broadened Argon Line Profiles

APPENDIX B

Charles F. Hooper, Jr.

DE-FG03-95SF20712

The Effects of Ion Dynamics and Opacity on Stark Broadened Argon Line Profiles

D. A. Haynes, Jr., D. T. Garber, C. F. Hooper, Jr.
University of Florida

R. C. Mancini
University of Nevada – Reno

Y. T. Lee
Lawrence Livermore National Laboratory

D. K. Bradley, J. Delettrez, R. Epstein, P. A. Jaanimagi
Laboratory for Laser Energetics

Abstracted Abstract

- We present the results of our theoretical and experimental investigation into the effecrts of **ion dynamics** and **opacity** on emission from Ar doped ICF plasmas.

- Our theoretical investgation led to the development of a density- and temperature-dependent spectrum modeling radiation in the spectral region 3500 – 4050eV from a uniform spherical Ar doped D_2 plasma, including emission from K- and L-shell Ar radiators.

- Our experimental investigation involved the study of several implosions at LLE on the pre-upgrade Omega, with Ar concentrations varying from 0.025% to 100%. Time resolved x-ray spectra were recorded.

- Comparison of the model spectrum to the experimental data led to an appreciation of the relative importance of ion dynamic and opacity effects as a function of Ar concentration. Also, the model spectrum proved a useful temperature and density diagnostic for Ar doped ICF implosions.

Abstract

We examine the combined effects of ion dynamics and opacity on line profiles used in the analysis of hot dense plasmas. Specifically, we have calculated Stark broadened line profiles for both resonance and satellite lines in highly stripped Ar ions, both in the quasi-static ion approximation, and including the effects of ion dynamics. Using the results of an NLTE kinetics code, combined with an escape factor formalism to account for the effects of radiative transfer, we have calculated the relative intensities of these lines, as well as the effects of opacity on their profiles. This model spectra is used in the analysis of experimental data.

In a series of experiments performed at the Laboratory for Laser Energetics plastic microballoons filled with DD and doped with Ar were imploded using the Omega laser system. Here, we will use time-resolved K-shell Ar spectra from the implosions. Varying the relative concentration of Ar in DD provides an opportunity to study the combined and individual effects of ion motion and opacity on the Stark broadened line profiles.

Stark Broadening

$$P_{a\to b} = \frac{4\omega_{ab}^4}{3c^3}|\langle a|\vec{d}|b\rangle|^2.$$

$$P(\omega) = \frac{4\omega^4}{3c^3}\sum_{a,b}\rho_a|\langle a|\vec{d}|b\rangle|^2\delta(\omega-\omega_{ab}).$$

$$I(\omega) = \sum_{a,b}\rho_a|\langle a|\vec{d}|b\rangle|^2\delta(\omega-\omega_{ab}).$$

$I(\omega)$ can be written

$$I(\omega) = \int d\vec{\mathcal{E}}\, Q(\vec{\mathcal{E}})J(\omega,\vec{\mathcal{E}}),$$

where

$$J(\omega,\vec{\mathcal{E}}) = -\frac{1}{\pi}\,\mathrm{Im}\,\mathrm{Tr}[\vec{d}\cdot R(\omega,\vec{\mathcal{E}})\rho\vec{d}]$$

and the trace is over the states of the radiating ion and the perturbing electrons, with the form of the resolvent $R(\omega,\vec{\mathcal{E}})$ depending on whether or not the **Quasi-static Ion Approximation** is used.

Quasi-static Ion Approximation

$$R(\omega, \vec{\mathcal{E}}) = [\omega - L_R(\vec{\mathcal{E}}) - M(\omega)]^{-1}$$

where $L_R(\vec{\mathcal{E}})$ is the radiator Liouville operator, including interaction with the plasma ion microfield, and $M(\omega)$ is the electron broadening operator, calculated in the relaxation approximation.

Ion-Dynamics

$$R(\omega, \vec{\mathcal{E}}) = \frac{\tilde{R}}{1 + i\nu(\omega) \int d\vec{\mathcal{E}} Q(\vec{\mathcal{E}}) \tilde{R}},$$

with

$$\tilde{R} = [(\omega + L_R(\vec{\mathcal{E}}) - M_e - i\nu(\omega)]^{-1},$$

and M_e the electron broadening operator calculated in the impact approximation, and ν a complex function of two parameters related to transport properties of the perturbing ions.

Static and Dynamic Ion Stark Broadening Calculations

Ar He-β

$n_e = 5 \times 10^{23}\text{cm}^{-3}$, $kT = 900\text{eV}$

0.025% Ar in D_2

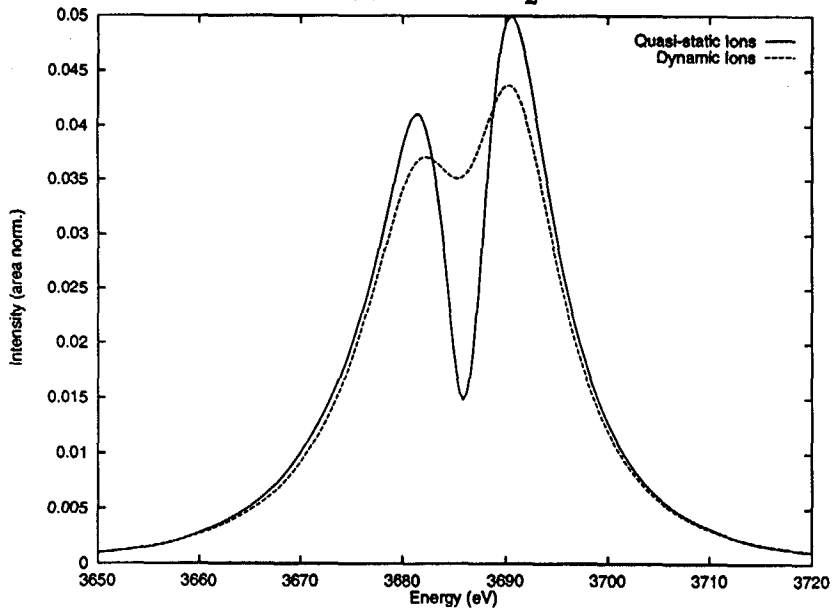

17% Ar in D_2

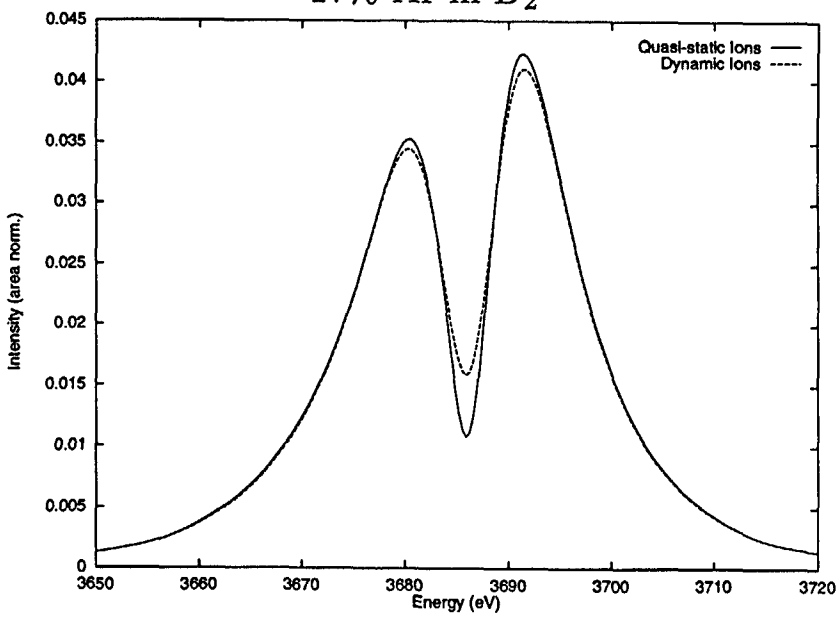

Dependence of Lineshape on Plasma Composition

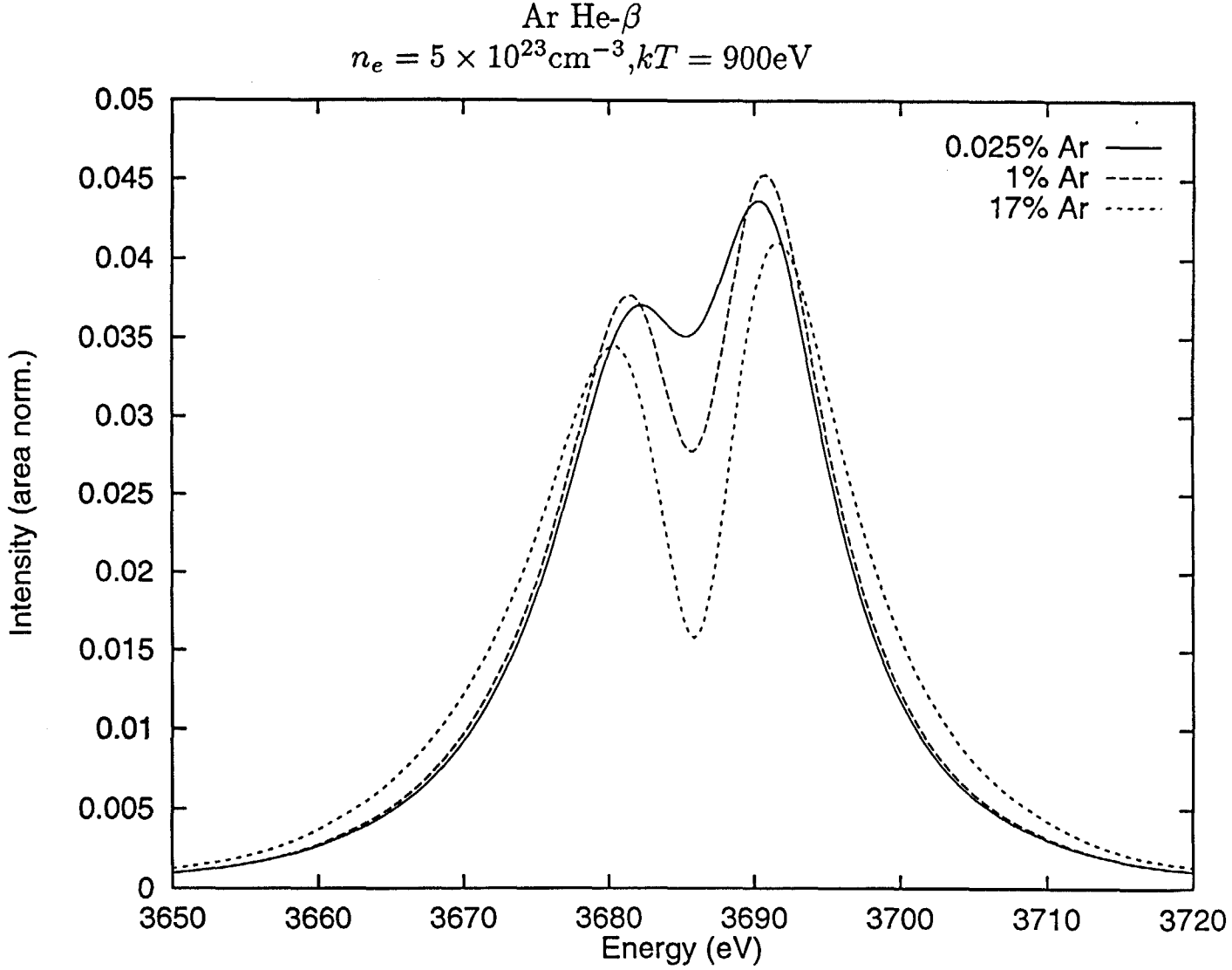

Opacity Effects on the Lineshape as a Function of Plasma Composition

$$\tau_\nu = \frac{\pi e^2}{mc} \bar{f} \hat{\varphi}_\nu N(\frac{2}{3}d)$$

Ar Ly-β

$n_e = 8 \times 10^{23}\text{cm}^{-3}$, $kT = 900\text{eV}$

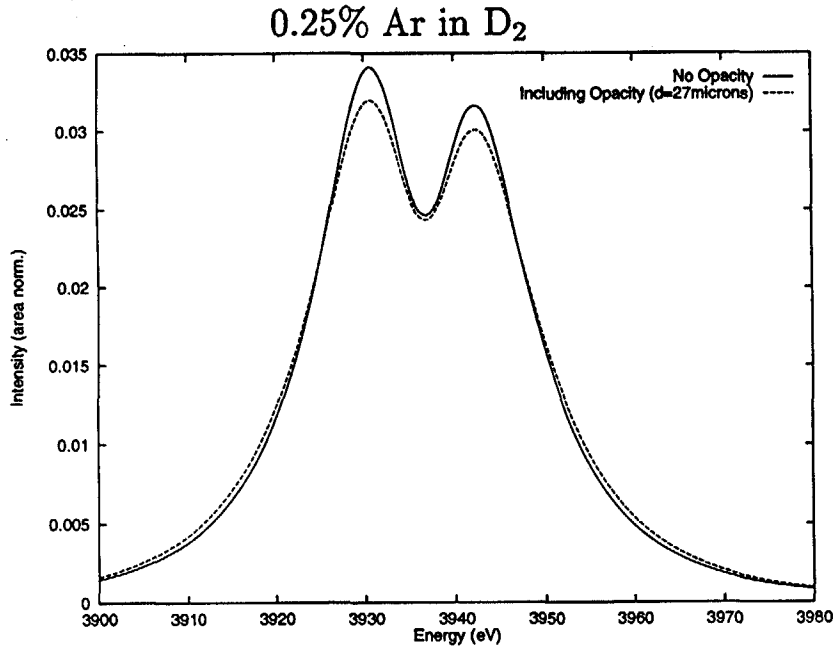

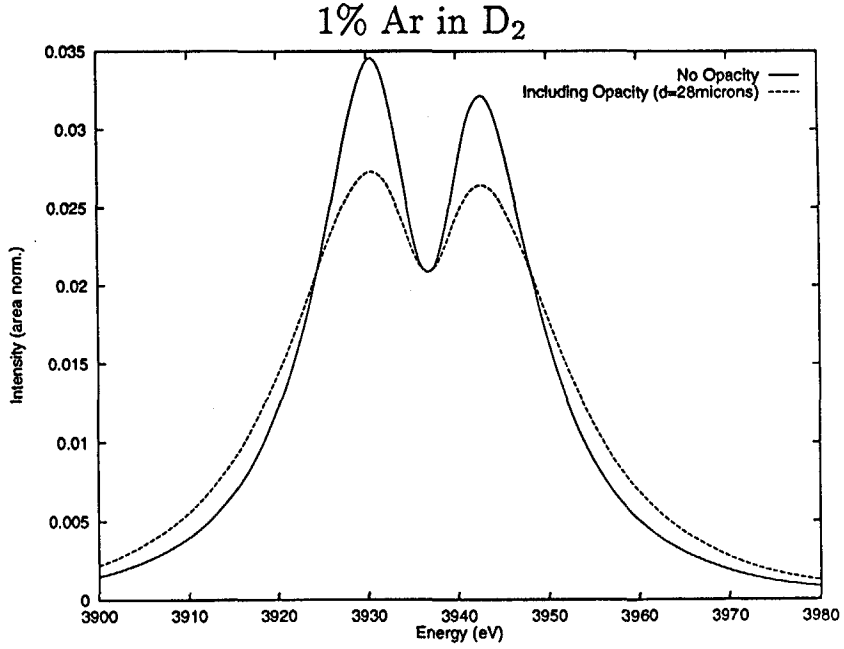

Ion Dynamics and Opacity Lineshape Effects

- For low concentrations of Ar in D_2, the usual Static Ion approximation in Stark broadening calculations is inadequate.

- As the concentration of Ar in D_2 increases, the increasing optical depths of the Ar emission lines modify the obseved lineshapes.

- A transition region exists, in which the lineshape near the peaks goes from being dominated by ion dynamics effects to being dominated by opacity effects. We investigate that region.

Combined Effects of Ion Dynamics and Opacity: 0.25% Ar and 1% Ar

Ar He-β, $n_e = 5 \times 10^{23}\text{cm}^{-3}$, $kT = 900\text{eV}$

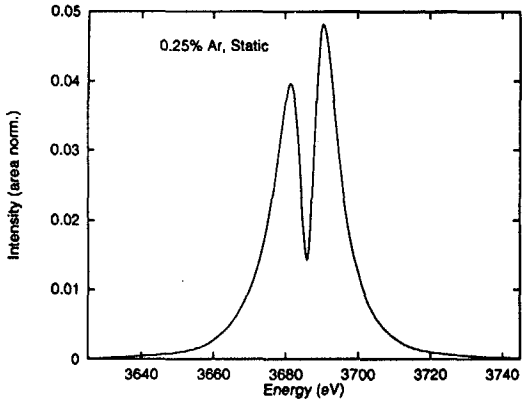

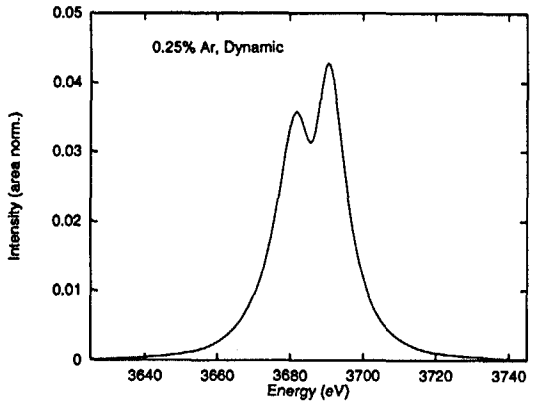

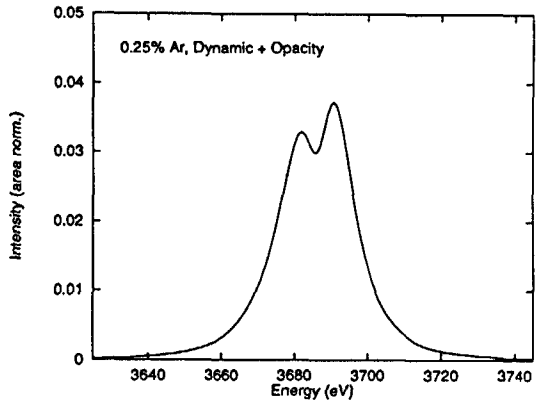

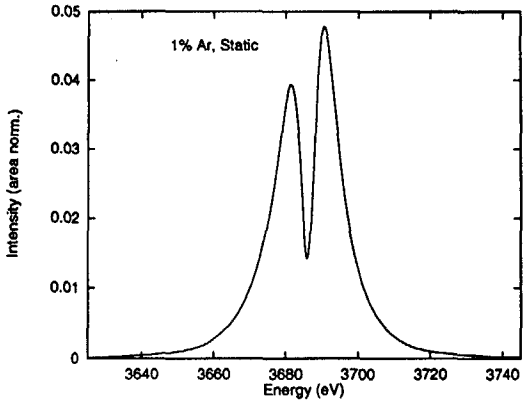

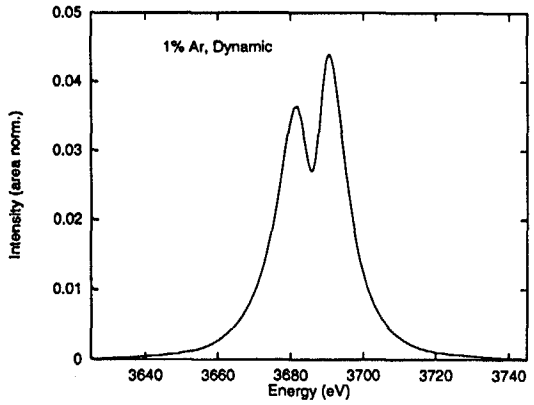

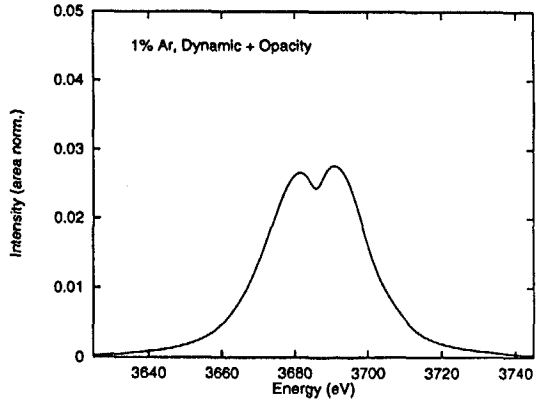

Development of Model Spectrum

- We model emission from a **uniform** spherical plasma, characterized by electron density, n_e, temperature, kT, and diameter d.
- Stark Broadened K- and L-Shell Ar line profiles, including the effects of ion dynamics
  - He-β, and Li-like satellites
  - He-γ, and Li-like satellite
  - He-δ
  - Ly-β, and He-like satellites
- Non-LTE populations
  - Optically thin kinetics model, with $\sim$ 1400 levels, with sufficient detail in the He- and Li-like ionization stages for detailed treatment of the satellites.
- Opacity effects
  - Opacity effects on the lineshape were approximated using a modified slab opacity formula.
  - The effects of radiative transfer on the relative intensities was calculated using density- and temperature- dependents escape factors calculated using the detailed Stark broadened lineshapes.

Optically Thin NLTE Results for Relative Intensities

Integrated Intensity Relative to Ar He-β

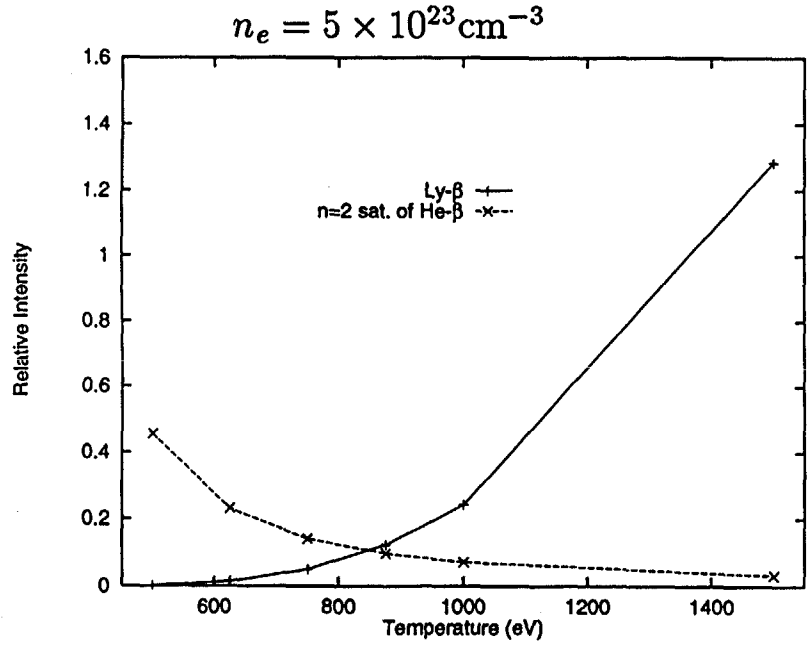

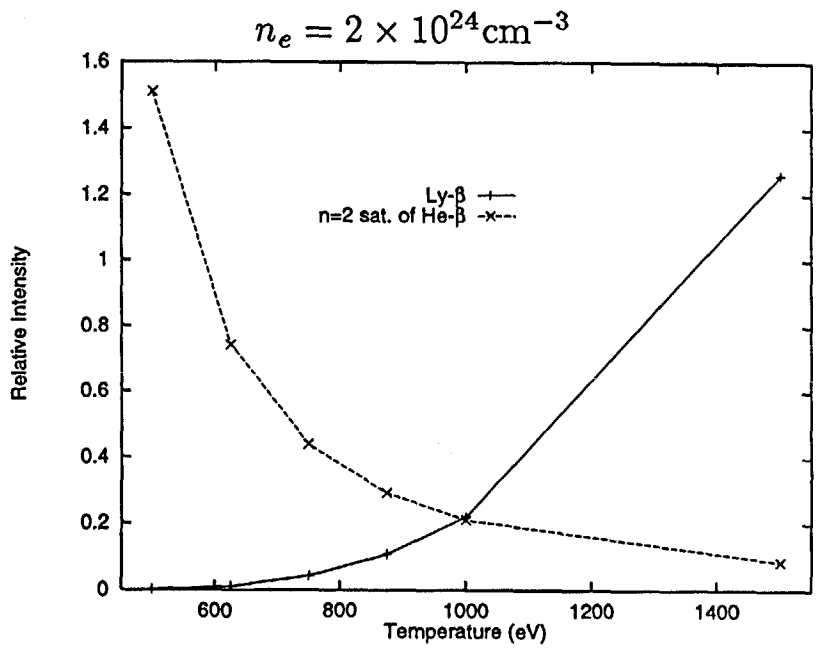

Modification of Relative Intensities Due to Radiative Transfer

$$C_x = \frac{I_x^{thick} / I_{Ly-\beta}^{thick}}{I_x^{thin} / I_{Ly-\beta}^{thin}}$$

$$n_e = 1 \times 10^{24} \mathrm{cm}^{-3}$$

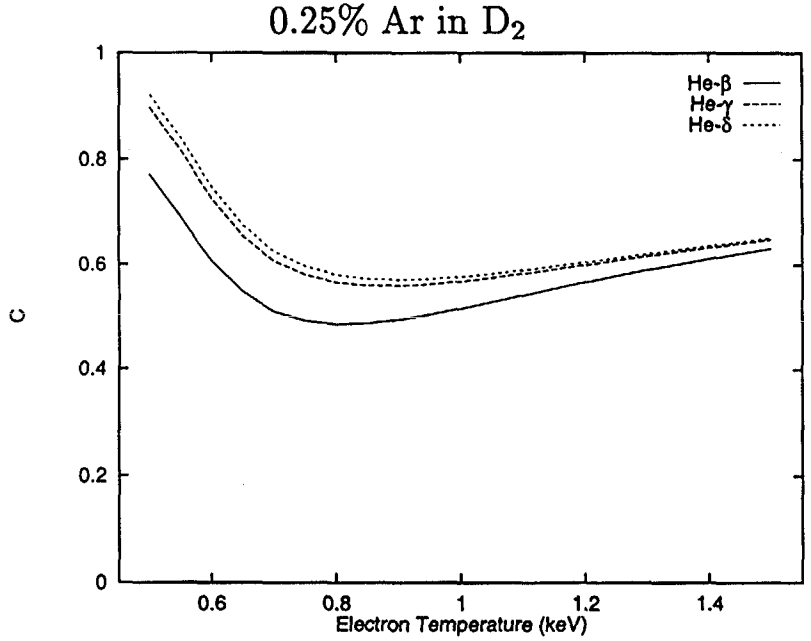

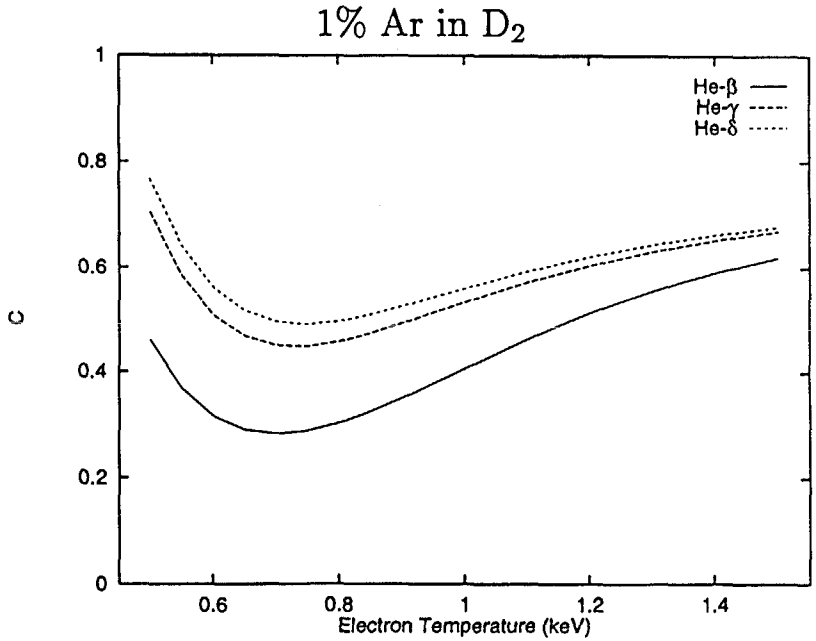

Density Dependence of the Model Spectrum

$kT = 900$eV, 0.25% Ar in D_2

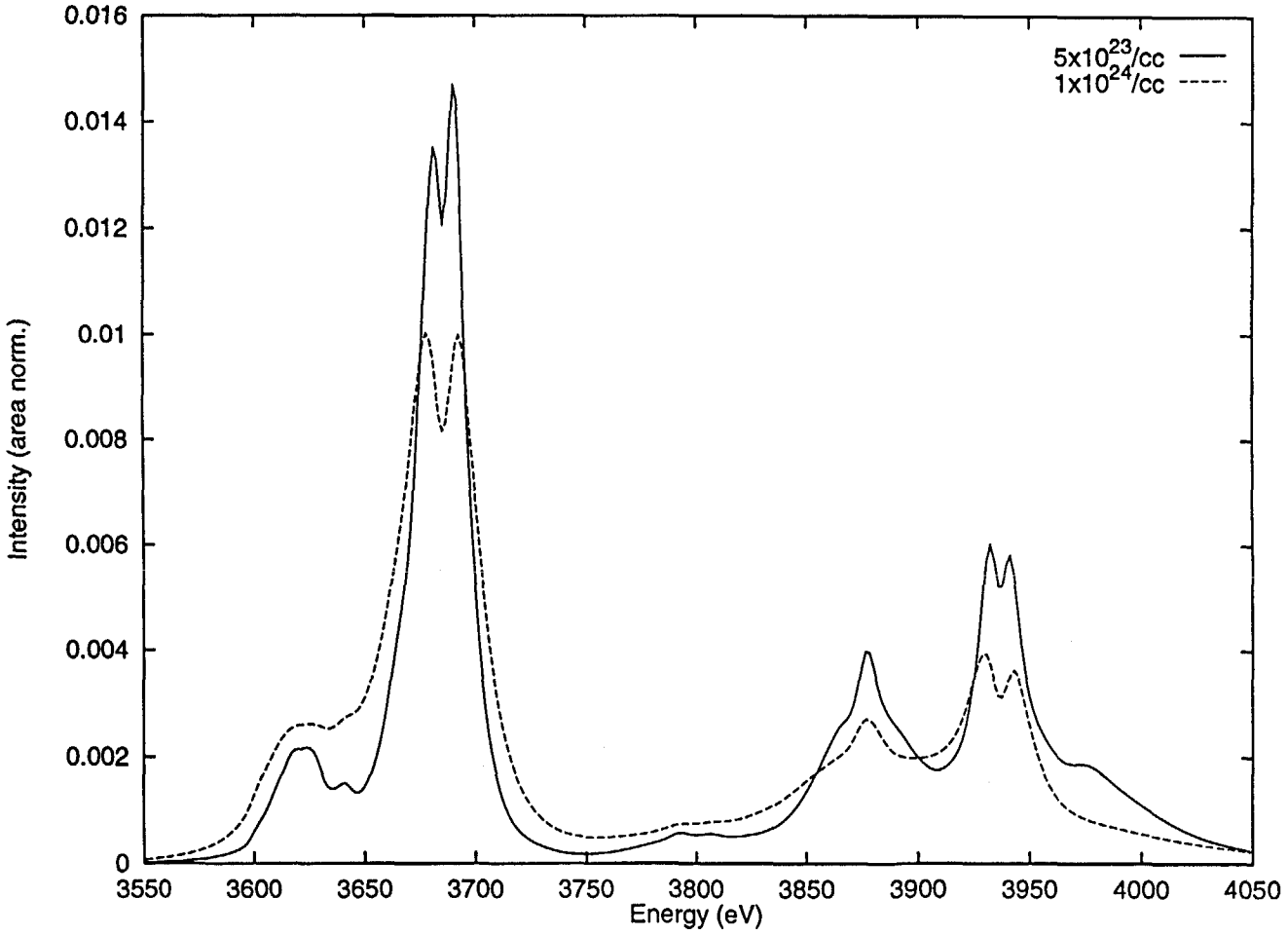

Temperature Dependence of the Model Spectrum

$n_e = 5 \times 10^{23}\text{cm}^{-3}$, 1% Ar in D_2

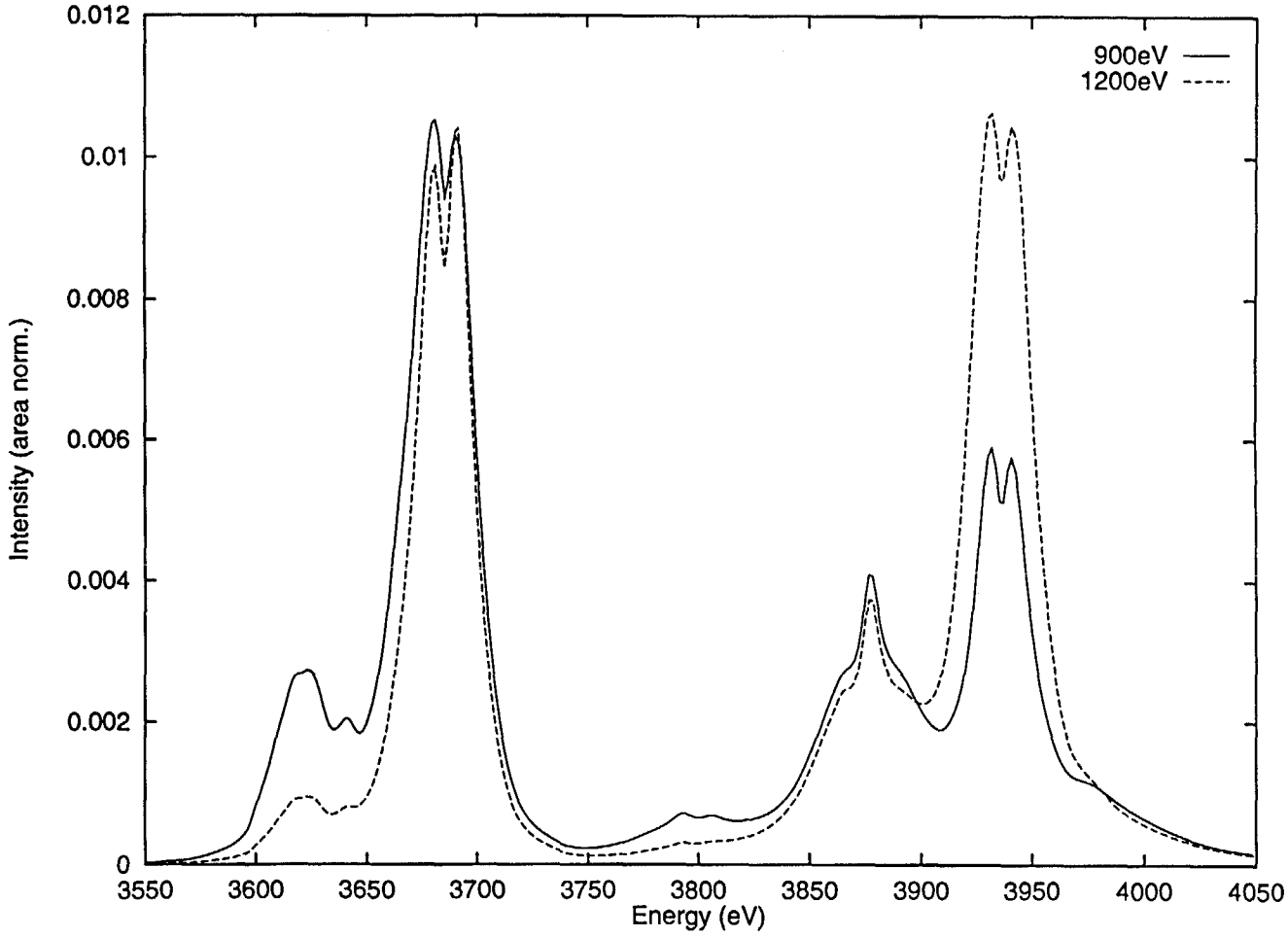

Ar Concentration Dependence of the Model Spectrum

$n_e = 5 \times 10^{23}\text{cm}^{-3}$, $kT = 900\text{eV}$

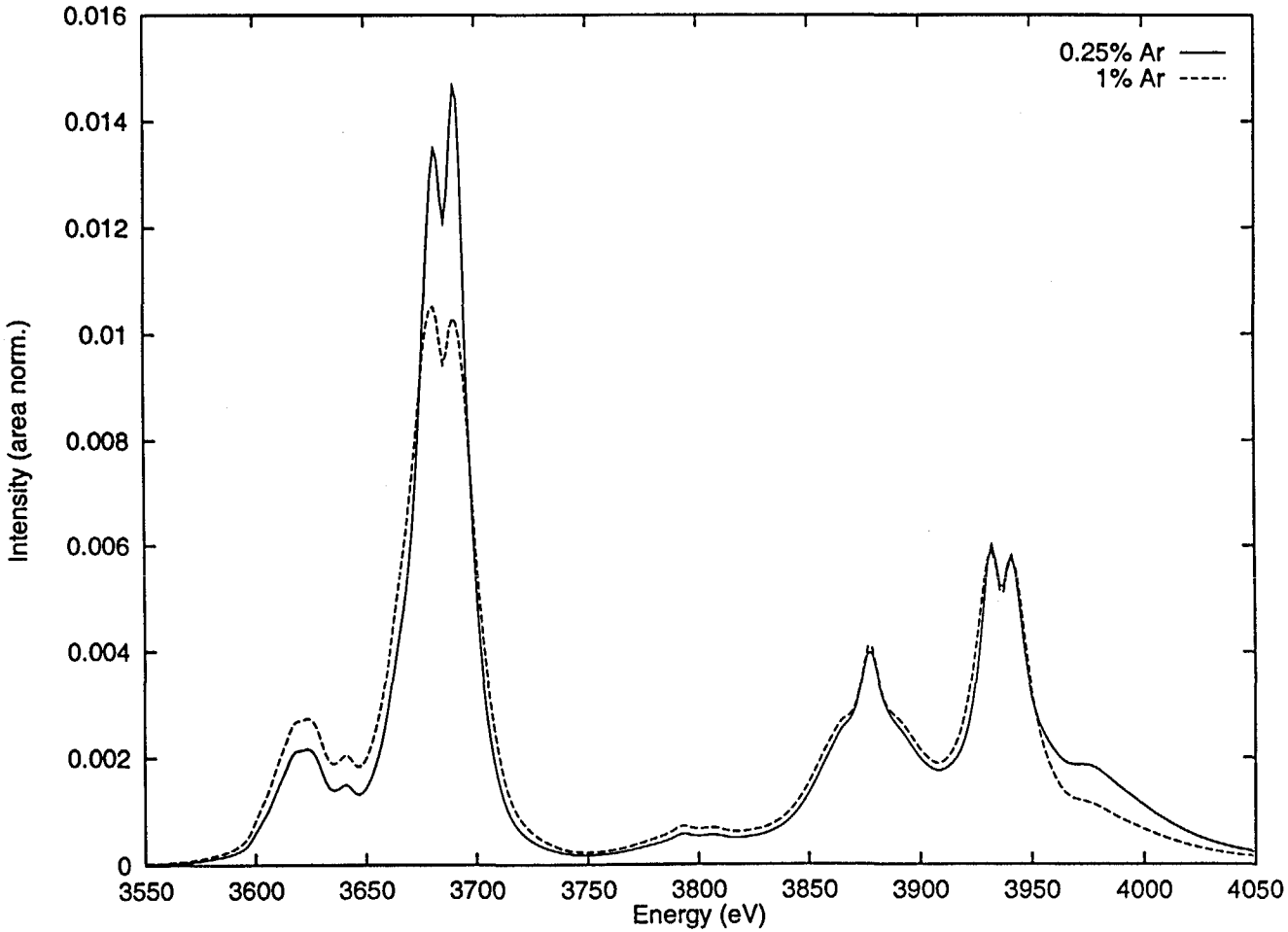

The Effect of Radiative Transfer on the Model Spectrum

$n_e = 1 \times 10^{24}\text{cm}^{-3}$, $kT = 900\text{eV}$, 1% Ar in D_2

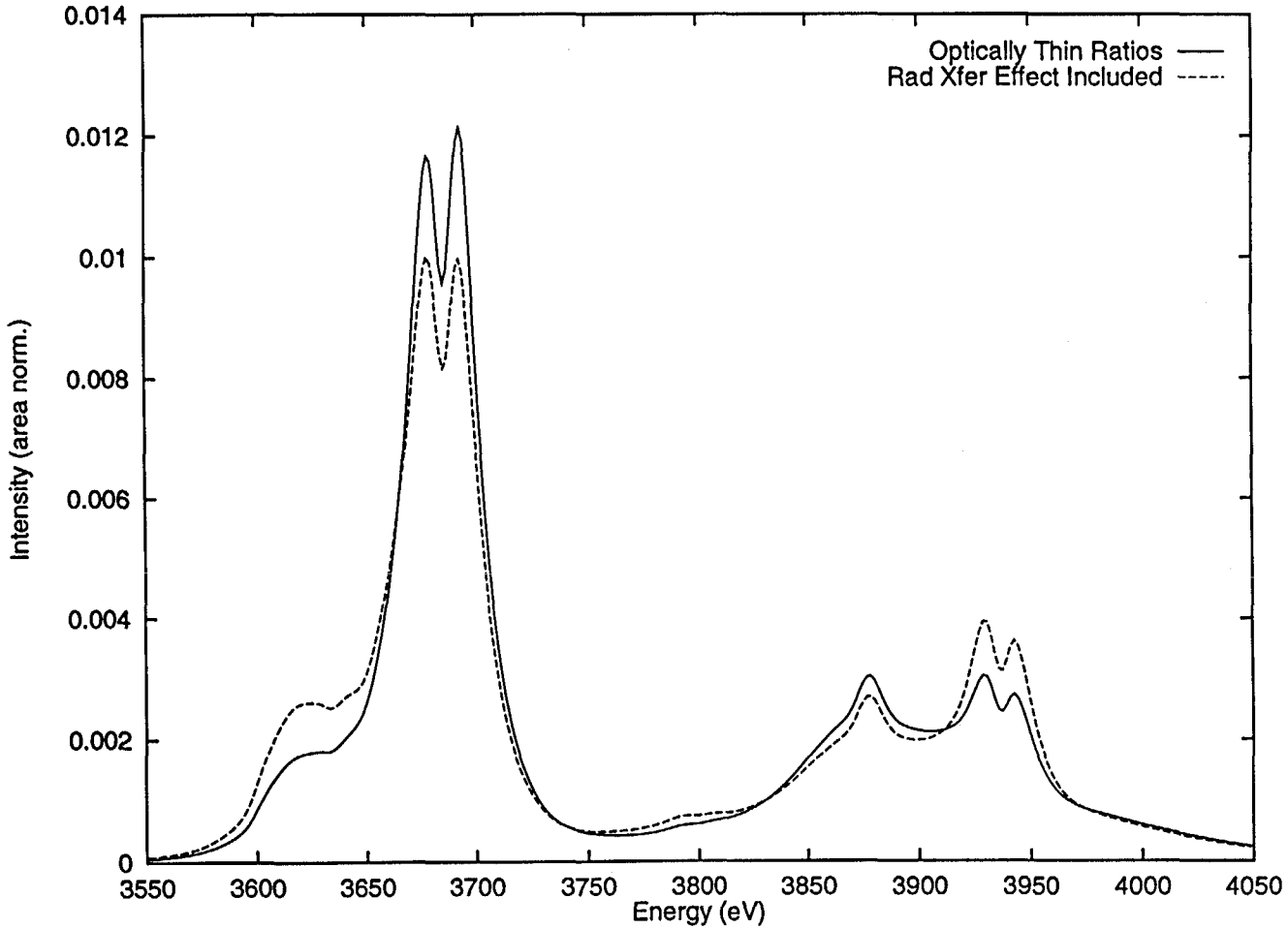

Experimental Data

- Targets: $\sim 250\mu m$ diameter microballoons, $6\mu m$ plastic shell, $0.05\mu m$ Al coating.
- Energy Absorbed: $\sim 600J$, 600ps pulse width.
- Gas fill: 20Atm combinations of Ar and D_2, with Ar concentrations ranging from 0.025% to 100%
- Time Resolved Spectrograph: Flat Crystal Spectrograph, ADP crystal with a 2-d spacing of 10.642Å coupled to an xray streak camera.
- Instrumental Response Function: Approximated as a gaussian with FWHM between 3.6eV (at 3680eV) and 4.4eV (at 3935eV).

Shot 24545 – 0.25% Ar in D_2: Time Resolved X-ray Data

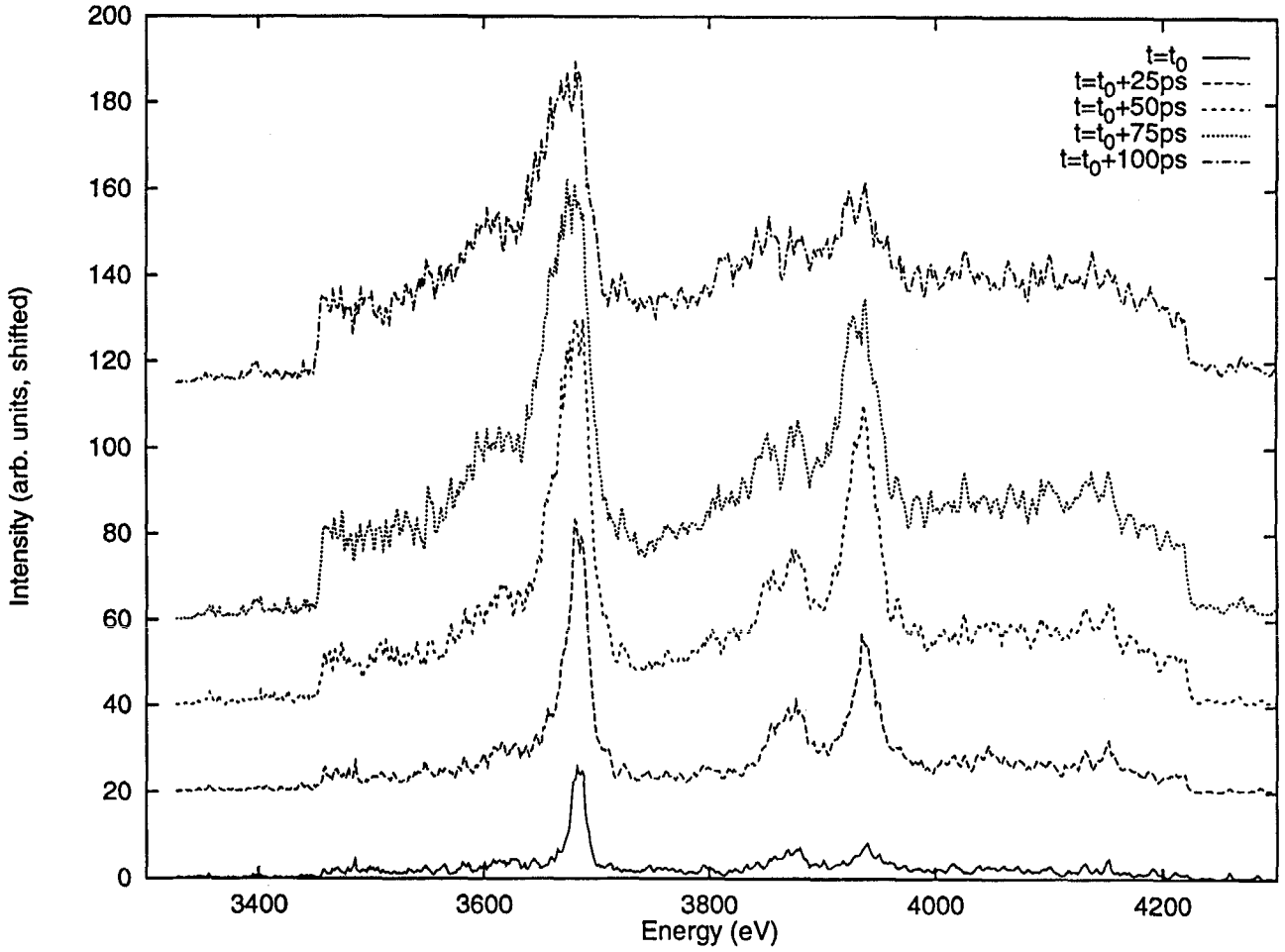

Shot 24542 – 1% Ar in D_2: Time Resolved X-ray Data

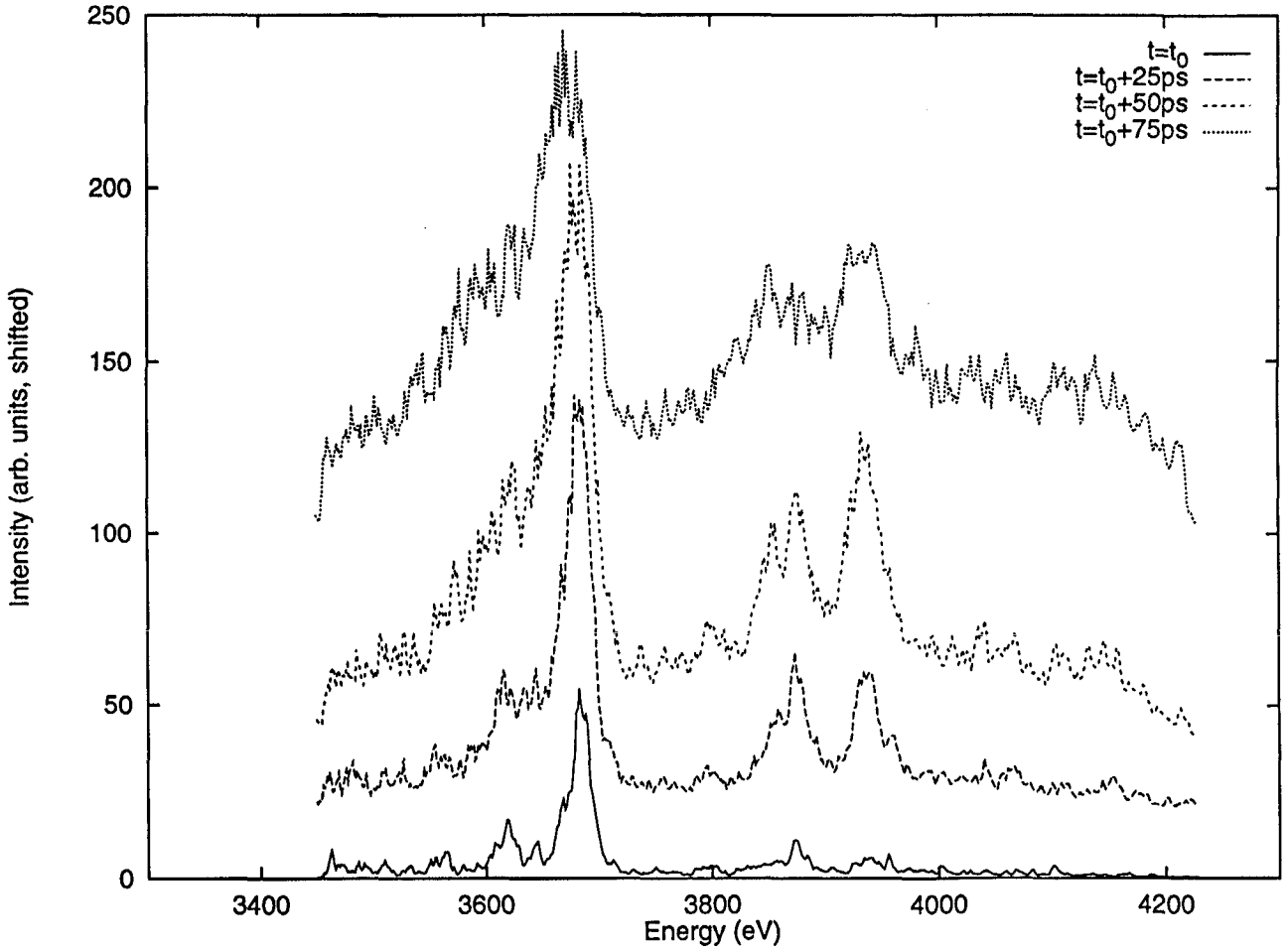

Goldilocks Shots

Time Integrated Data

Shot 24544 – 0.025% Ar in D_2

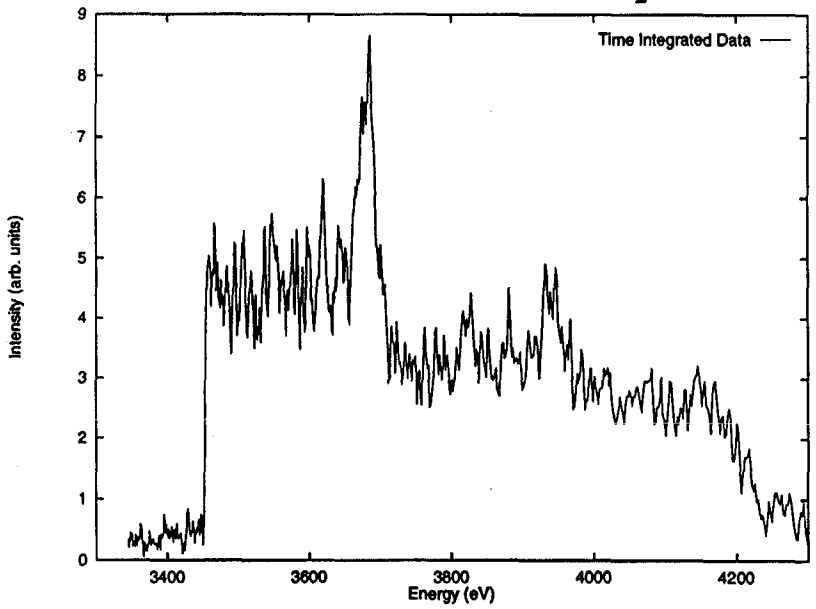

Shot 24543 – 33% Ar in D_2

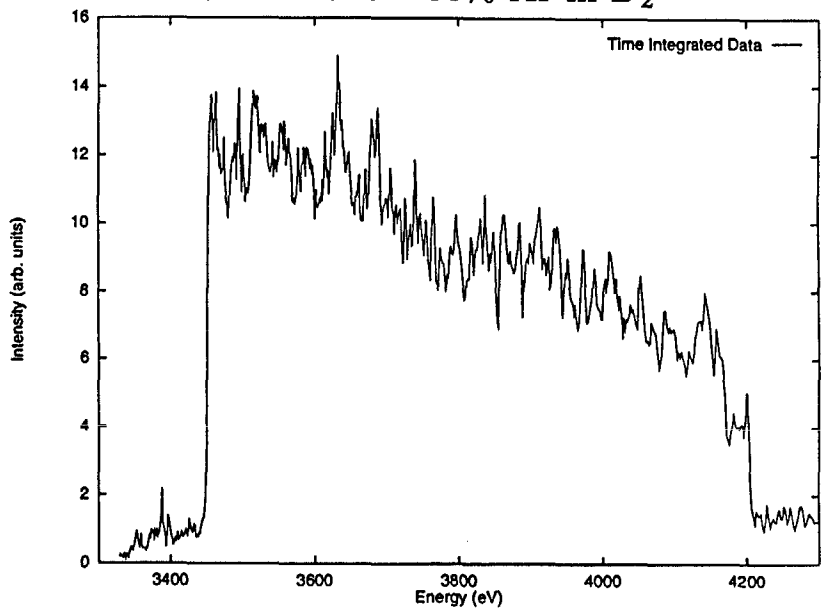

Analysis of Hot Dense Plasmas: 0.25% Ar in D_2

$$n_e = 8 \times 10^{23} cm^{-3},\ kT_e = 925eV$$

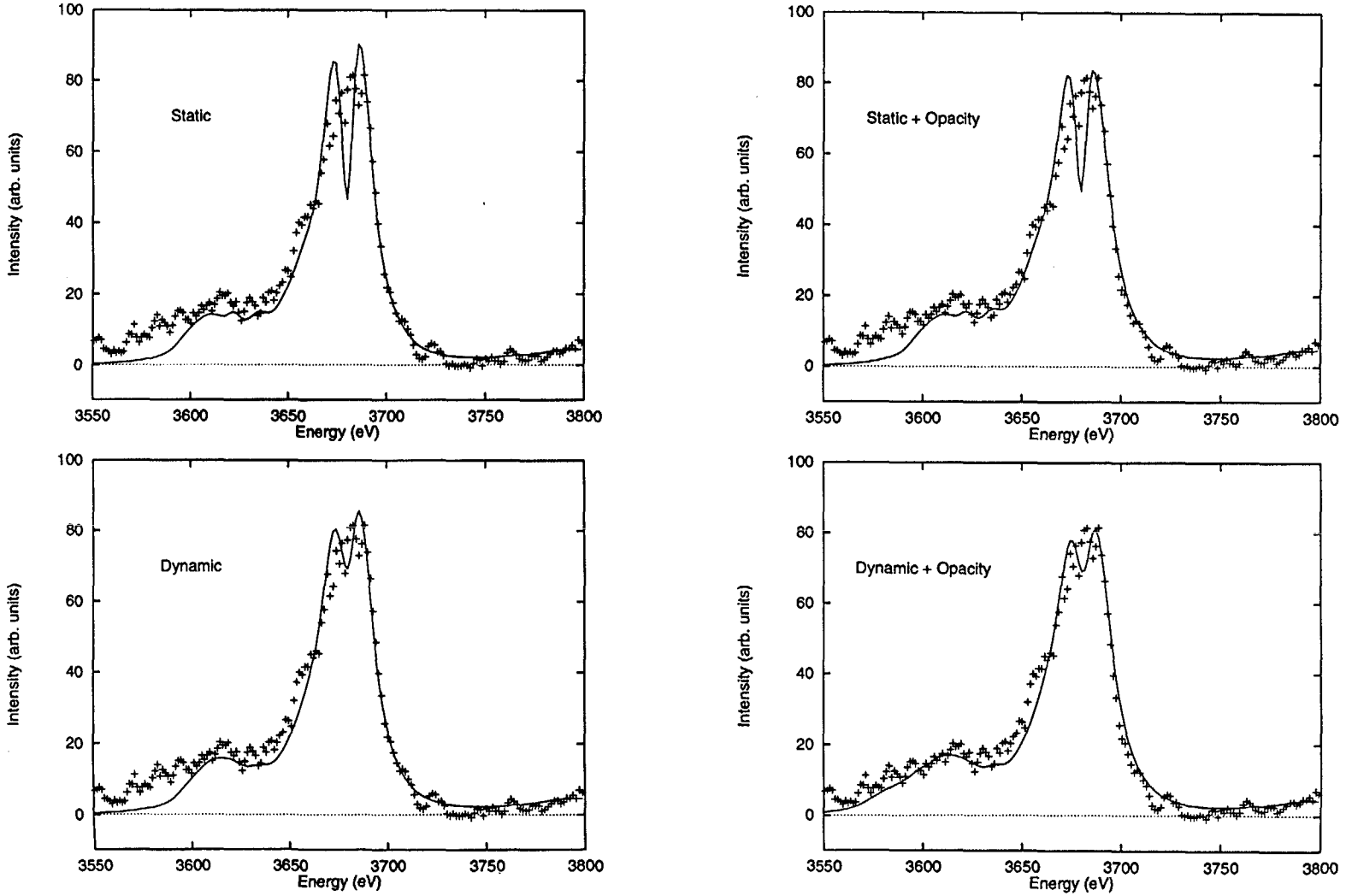

Analysis of Hot Dense Plasmas: 1% Ar in D_2

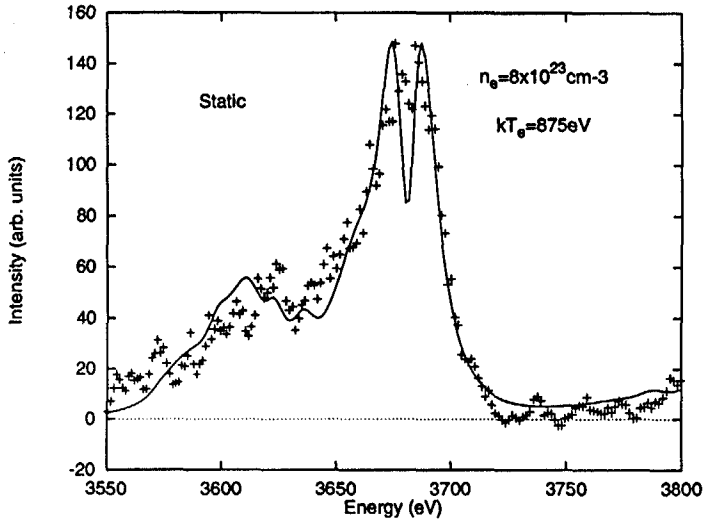

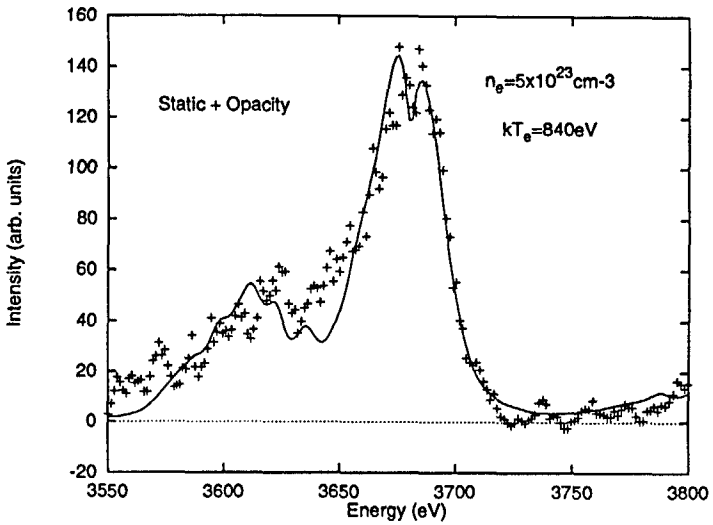

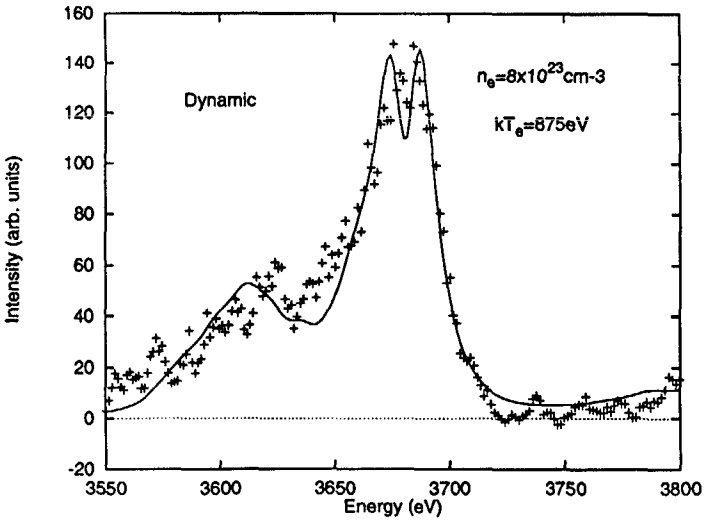

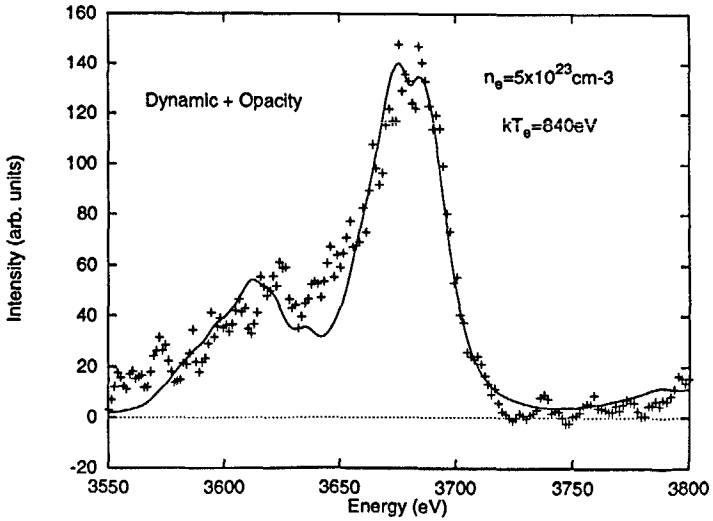

Analysis of Hot Dense Plasmas: 1% Ar in D_2

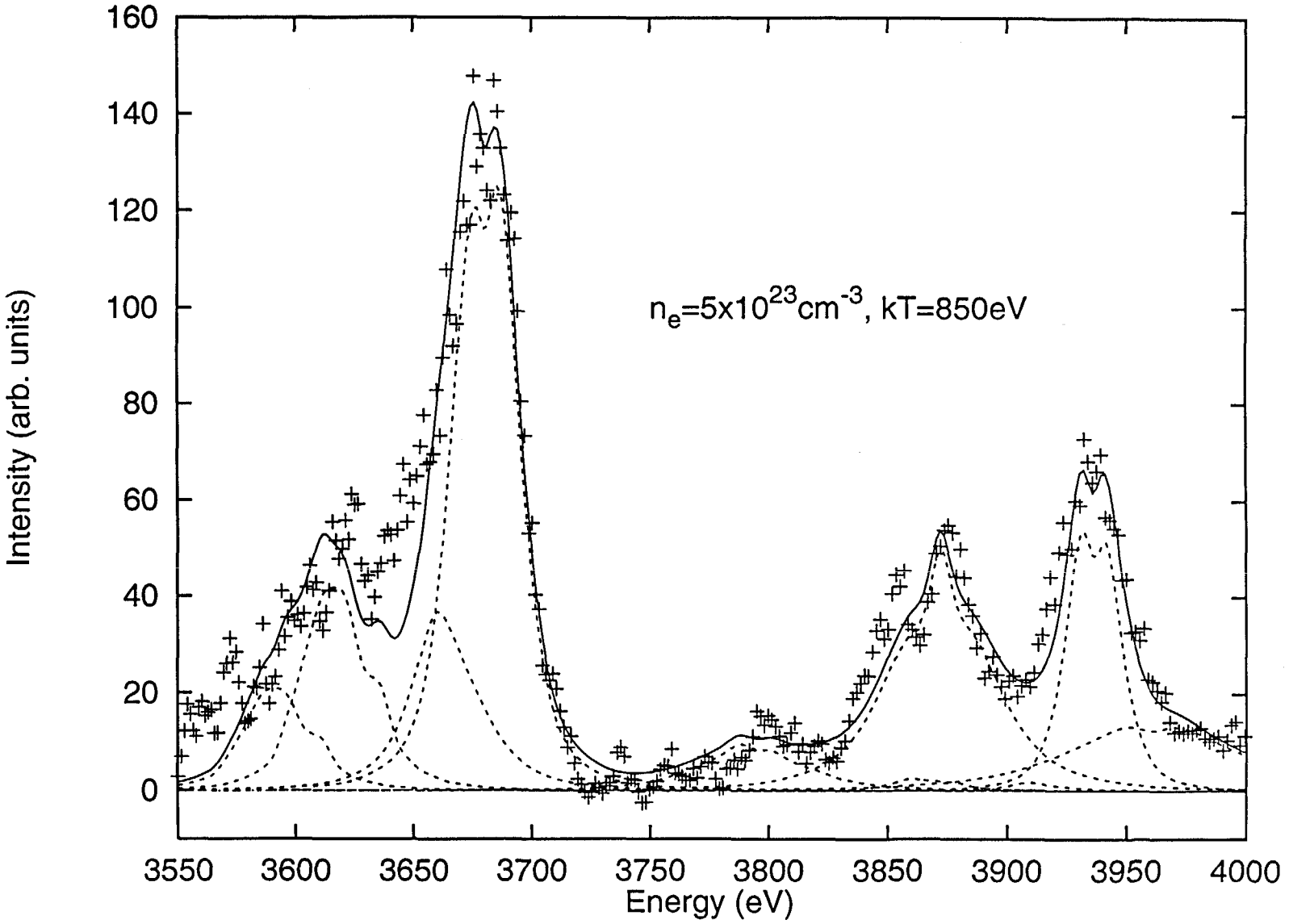

Conclusions

- Ion dynamics and opacity effects lead to modifications of Ar resonance lines which are particularly apparent at the dip in the β lines.

- We can fit experimental data with little, if any, apparent dip at the center of the He-β, with the dip being "filled in" by a combination of ion dynamics and opacity effects, depending on the relative concentration of Ar in D_2.

- Our model spectrum displays diagnostically useful temperature and density sensitivity, and adequately fits the time resolved x-ray spectra from these experiments.

- The effects of **gradients** in the core structure can also lead to modifications of the lineshapes. (See, *e.g.*, Leng, Goldhar, Griem, and Lee Phys. Rev. E **52** 4328 (1995).)

References

- Stark Broadening Calculations
  - Thor Garber's poster, this conference.
  - Mancini, Kilcrease, Woltz, and Hooper, Comp. Phys. Commun. **63**, 314 (1991).
  - Boercker, Iglesias, and Dufty, Phys. Rev. A **36**, 2254, (1987).
- Opacity Effects
  - Delameter, *et al.*, Phys. Rev. A **31**, 2460 (1985).
  - Mancini, Joyce, and Hooper, J. Phys. B **20**, 2975 (1987).
- NLTE Kinetics
  - Lee, J. Quant. Spectrosc. Rad. Trans. **38**, 131 (1987).

reprint, pp 6